doi:10.1016/j.jmb.2004.09.094 J. Mol. Biol. (2004) xx, 1–8

JMB

Available online at www.sciencedirect.com

SCIENCE DIRECT®

ELSEVIER

COMMUNICATION

Crystal Structure of the Spindle Assembly Checkpoint Protein Bub3

Nicholas A. Larsen[1] and Stephen C. Harrison[2]*

[1]*Department of Biological Chemistry and Molecular Pharmacology, Harvard Medical School, Boston, MA USA*

[2]*Howard Hughes Medical Institute, 250 Longwood Ave Boston, MA 02115, USA*

**Corresponding author*

Bub3 is one of at least six proteins that transmit the spindle assembly checkpoint signal. These proteins delay cell cycle progression from metaphase to anaphase in response to attachment defects between kinetochores and spindle microtubules and to tension defects between sister chromatids. To explore the molecular interactions mediated by Bub3, we have determined the crystal structure of the *S. cerevisiae* protein Bub3p at 2.35 Å resolution. Bub3p is a seven-blade β-propeller, although its sequence diverges from that of other WD40 family members. Several loops are substantially elongated, but extra domains or insertions are not present at the termini. In particular, two extended loops project from the top face of the propeller, forming a cleft. Amino acid residues across the top face and one aspect of the lateral surface (spanning blades 5–6) are highly conserved among Bub3 proteins. We propose that these conserved surfaces are the loci for key interactions with conserved motifs in spindle checkpoint proteins Bub1 and Mad3/BubR1. Comparison of the Bub3 sequence to the WD40 protein, Rae1, shows high sequence conservation along the same surfaces. Rae1 interaction with Bub1 is, therefore, likely to involve a similar mode of binding.

Keywords: spindle checkpoint; bub3; bub1; mad3; kinetochore

The kinetochore is a multi-protein scaffold that assembles on centromeric DNA and establishes a connection with the mitotic spindle. Bipolar attachment of sister kinetochores to spindle microtubules is necessary for progression from metaphase to anaphase; a single unattached kinetochore is sufficient to delay the cell cycle.[1,2] Activation of the spindle checkpoint generates the delay signal (reviewed by Yu),[3] and defects in checkpoint control result in chromosomal instability. Current models posit that the delay signal is generated catalytically at unattached kinetochores and diffuses thence throughout the cytoplasm to inhibit the anaphase promoting complex.[3] The specific molecular mechanisms for detecting attachment and tension defects are still obscure.

Bub3 is not an essential gene in budding yeast, although bub3Δ cells grow slowly and do not arrest in response to the spindle poison nocodazole.[4] Bub3 is essential in higher eukaryotes.[5,6] Co-immunoprecipitation and co-fractionation experiments, from extracts of both budding yeast and higher eukaryotic cells, show that Bub3 forms at least two tightly bound, constitutive protein subcomplexes throughout the cell cycle: Bub1–Bub3 and Mad3/BubR1–Bub3.[7–10] (Note the Mad3 ortholog in higher eukaryotes is BubR1.) Bub1 is a non-canonical kinase[11] with a distinctive amino-terminal regulatory domain that has sequence similarity to parts of Mad3/BubR1. In particular, Mad3/BubR1 and Bub1 share a motif of about 45 amino acid residues, which has been shown by co-immunoprecipitation and yeast two-hybrid analysis to be necessary for binding to Bub3.[8,9] Moreover, Bub3 is a component of the cell-cycle regulated mitotic checkpoint complex, comprising Mad3/BubR1–Bub3–Mad2–Cdc20, which inhibits activation of the anaphase promoting complex.[9,10,12–14] Fluorescence microscopy and chromatin immunoprecipitation experiments show that Bub3 co-localizes with Bub1 and Mad3/BubR1 at unattached kinetochores.[8,15–17] The precise nature of these interactions at the kinetochore is unknown, although genetic data suggest that two proteins in the Ndc80 complex, Spc24 and Spc25, may be important.[17–19]

Abbreviations used: ALS, advanced light source; MCC, mitotic checkpoint complex.

E-mail address of the corresponding author: schadmin@crystal.harvard.edu

In addition, the entire Ndc80 heterotetramer is necessary for spindle checkpoint proteins Mad1/Mad2 interaction at the kinetochore.[19–21] Unattached kinetochores appear to bind only a small fraction of the cytoplasmic population of checkpoint proteins, and the kinetochore-bound checkpoint proteins exchange with diverse kinetics.[22,23]

A network of protein–protein interactions has thus been identified for Bub3, but the question of how these interactions conspire to generate the delay signal remains. We present here the crystal structure of Bub3 from *S. cerevisiae* (Bub3p) as a step towards a structural understanding of its role.

Purification and crystallization of Bub3p

The bub3 gene from *S. cerevisiae* was amplified from a genomic library and subcloned into pET-22b(+) (Novagen), in-frame with the vector encoded, C-terminal His_6-tag. Se-Met substituted Bub3p was overexpressed in BL834(DE3) methionine auxotroph cells (Novagen) by overnight induction at 23 °C. Soluble Bub3p was purified from bacterial lysate by Ni-NTA chromatography (Qiagen) followed by size exclusion chromatography on an S200 16/60—Sephadex column (Pharmacia) equilibrated in 250 mM NaCl, 10 mM Tris pH 8.0, and 10 mM β-mercaptoethanol. The protein eluted at a volume corresponding to the expected molecular mass of 38 kD. The peak fractions were pooled and concentrated to 13 mg ml^{-1} in the presence of 10 mM DTT.

Optimized Bub3p crystals grew overnight from 20–24% (w/v) PEG 3350, and 100 mM citrate pH 5.4–5.8. They were frozen after immersion in a 20% (v/v) glycerol substituted cryo-protectant. The largest (~40 μm × 40 μm × 20 μm) gave sharp diffraction (mosacity 0.35°) at the Advanced Light Source (ALS) beam-line 8.2.1. SAD and MAD data were collected at 2.35 Å, and 2.6 Å, respectively, from two separate crystals (Table 1). The data were processed using HKL2000,[24] initially in space group $P321$ with $a=b=73$ Å, $c=110$ Å, and a calculated solvent content of 46%, assuming a single molecule per asymmetric unit.

Structure determination

There are three methionine residues, including the amino terminus, in Bub3p. All three were sufficiently ordered to obtain phases and an interpretable electron density map for the entire molecule in space group $P3_221$. Initial sites were obtained from the MAD data using SOLVE[25] and refined using SHARP.[26] The phases were extended to the higher resolution limit of the SAD data using solvent flipping and flattening procedures implemented by SOLOMON[27] and DM.[28] The resulting electron density map was of sufficient quality to trace manually 290 of 340 residues in O[29] and the three methionine residues and aromatic side chains served as anchor points for subsequent docking of 270 residues of the sequence. These initial model phases were combined with the experimental phases in CNS[30] to calculate a new map, from which the remaining model could be traced.

Table 1. Data and refinement statistics

	SAD λ1 (f″)	MAD λ1 (f″)	MAD λ2 (f′)	MAD λ3
Wavelength	0.9795	0.9795	0.9796	0.9200
Resolution[a]	2.35 (2.39–2.35)	2.60 (2.64–2.60)	2.60 (2.64–2.60)	2.70 (2.75–2.70)
Space group	$P3_2$	$P3_221$	$P3_221$	$P3_221$
Unique obs.	52,125	18,726	18,776	16,107
Redundancy[a]	2.9 (2.9)	3.8 (3.7)	3.8 (3.6)	3.8 (3.5)
Completeness[a]	94.6 (93.2)	91.9 (95.5)	91.9 (94.5)	88.6 (93.3)
R_{sym}[b]	5.7 (48.8)	5.7 (50.0)	5.8 (50.7)	5.8 (40.0)
I/σ[a]	19 (1.7)	18 (1.7)	18 (1.7)	18 (2.1)
Refined residues		656		
Refined water molecules		349		
R_{cryst}[c]		19.6%		
R_{free}[d]		28.8%		
Average B-values (Å^2)				
Bub3		59		
Water molecules		53		
R.m.s. deviations from ideal geometry				
Bond lengths		0.0074 Å		
Bond angles		1.4°		
Dihedral angles		25.7°		
Improper angles		0.8°		

[a] Numbers in parenthesis refer to the highest resolution shell.

[b] $R_{sym} = [\sum_h \sum_i |I_i(h) - \langle I(h)\rangle| / \sum_h \sum_I I_i(h)] \times 100$, where $\langle I(h)\rangle$ is the average intensity of i symmetry related observations of reflections with Bragg index h.

[c] $R_{cryst} = [\sum_{hkl} |F_o - F_c| / \sum_{hkl} |F_o|] \times 100$, where F_o and F_c are the observed and calculated structure factors.

[d] R_{free} was calculated as for R_{cryst}, but on 5% of data excluded before refinement.

Evidence for crystal twinning

The refinement in CNS stalled with $R=27\%$ and $R_{free}=32\%$ after eight iterative rounds of careful rebuilding and refinement (water molecules included). Subsequently, the data were analyzed for merohedral twinning in the lower symmetry space group $P3_221$, according to the standard diagnostic intensity distributions $\langle H\rangle=0.03$ and $\langle H^2\rangle=0.003$.[31] These values suggested twinning with a twin fraction of 0.46 and a twinning operator coincident with the NCS operator (the crystallographic dyad in $P3_221$) $h, -h\ -k, -l$. SHELXL allows simultaneous refinement of the structure and the twinning fraction.[32–34] The resulting sigma weighted maps revealed clear differences in the electron density between the two molecules in the asymmetric unit, especially in the flexible loop regions.

Refinement of the Bub3p structure

The structure of Bub3p was determined to 2.35 Å resolution with $R_{cryst}=19.6\%$ and $R_{free}=28.8\%$ and a refined twinning fraction $\alpha=0.49$ (Table 1). Two molecules were refined in the asymmetric unit; they were nearly identical with each other, with a backbone C^{α} root-mean-squared difference (rmsd) of 0.7 Å. The main differences between the two molecules were in the loops, where one had two disordered regions (residues 226–231 and 322–324), while the other had three (residues 181–183, 226–231, and 243–248) (Figure 1). In addition, the restriction site sequence (LE) and His_6 tag were disordered in both molecules. The challenges encountered in building and refining the loop regions betray their inherent flexibility, which may be still greater in solution when free from crystal-packing constraints.

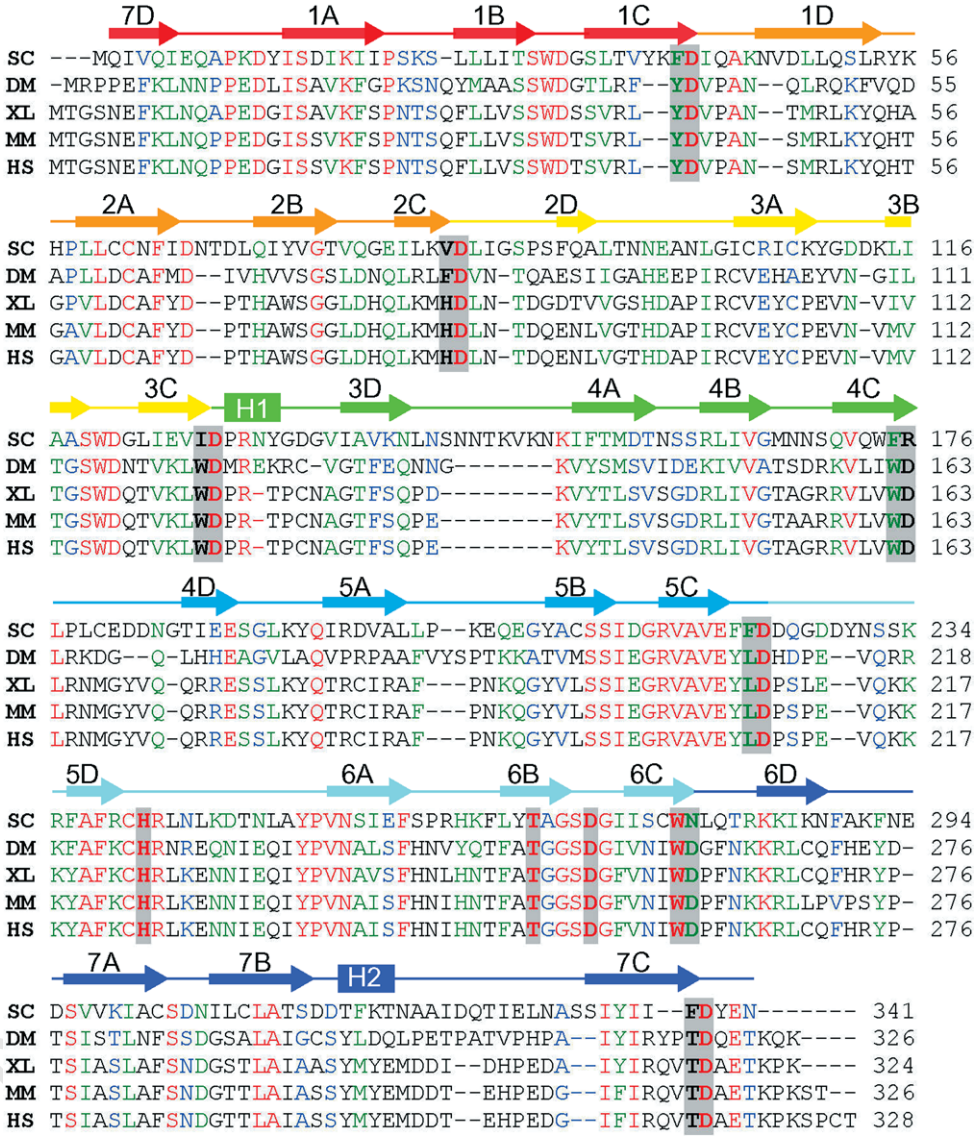

Figure 1. Annotated structural sequence alignment of Bub3. The primary sequence of bakers yeast (SC) was aligned with known bub3 homologs from Drosophila (DM), Xenopus (XL), mouse (MM), and Human (HS) using CLUSTALW.[44] Residues in the sequence are color coded according to their similarity. The coloring scheme of the annotated secondary structure will be followed in subsequent figures. Highlighted residues correspond to the WD signature sequence, which in Bub3p is highly divergent. The residues in the conserved structural triad in blade 6 are also highlighted.

Structural overview

The crystal structure shows that Bub3p is a canonical seven-bladed β-propeller (Figure 2(a)). The presence of WD40 repeats had been recognized from its sequence,[8,10] but there has been disagreement about their number. Each blade is a β-sheet of four anti-parallel strands, with strand order βA, βB, βC, βD. The β-sheets are arranged in pseudo-sevenfold rotational symmetry about a central axis with βA nearest the axis and βD furthest (Figure 2(a)). The top surface of the propeller is defined by the BC loops that join βB and βC within each blade and the DA loops that join βD and βA of consecutive blades. The bottom face is defined by AB and CD loops that join βA with βB and βC with βD, respectively (Figure 2(b)). The WD40 repeat, as conventionally defined from the amino acid sequence, does not correspond to a single blade in the tertiary structure, but rather spans two blades. The primary-sequence repeat begins with βD of blade "n" and ends with the signature sequence WD at the end of βC of blade "$n+1$". In order to complete this pattern, βD in blade 7 is derived from the amino-terminal strand, linking the first and last blades of the propeller (Figure 2(a)). The width of Bub3p from the top face to the bottom face is ~27 Å; the diameter is ~42 Å. The blades surround a central, water-lined channel that is wider near the bottom face and tapers slightly near the top face (~18 Å *versus* ~14.5 Å C^{α} to C^{α}).

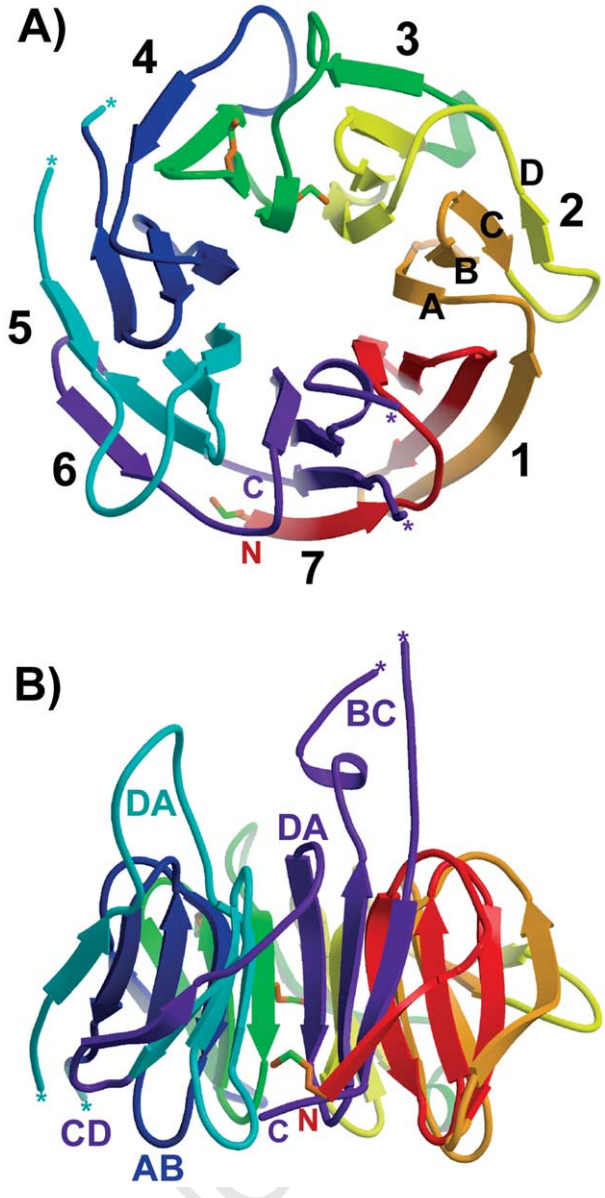

Figure 2. Top/side views of Bub3. (A) The top view shows the overall topology. Note that any given sequence repeat spans two blades, forming βD in blade "$n-1$" and βA–βC in blade "n". The three Se-methionine residues (sticks) are shown. Stars indicate disordered loop regions that were not traceable. (B) A 90° rotation relative to the top view, illustrating the relative height of the DA loop between blades 5 and 6 as well as the BC loop in blade 7. The figure was generated in Bobscript[45] and rendered with Raster3d.[46]

Structural divergence of the blades

WD40 proteins have diverse cellular functions, from signal transduction at the plasma membrane to transcriptional regulation in the nucleus. The amino acid sequence of Bub3p has only 11–16% sequence identity to those of other WD40 proteins of known structure. Nonetheless, structural comparison of Bub3p to the other known WD40 structures, using the DALI algorithm,[35] shows a significant degree of structural conservation, with an rmsd for related elements that ranges between 2.5 Å and 3.7 Å. Indeed, the core β-sheets of most of these proteins superimpose very well, with major differences occurring only in the more flexible loops regions and at the N and C termini, where insertions frequently occur (Figure 3(a)).

In the prototype WD motif, the Trp of the signature sequence (at the end of βC) packs between blades "n" and "$n-1$" and forms conserved hydrogen bonds in a triad involving Ser/Thr, His, and Asp (Figure 3(b)). In Bub3p, the WD signature sequence is largely absent, with blades 1–7 terminating in FD, VD, ID, FR, FD, WN, and FD, respectively (Figure 1). These divergences influence core contacts between blades. The only element of the prototypic structural triad that is conserved in Bub3p is the Asp/Asn/Gln at the tip of the BC loops, but its side chain has different interactions in different blades. Only blade 6 contains the classic Trp, Ser, Asp and His residues; these are conserved in all Bub3 homologs (Figures 1 and 3(b)). The lack of the structural triad in all but this one blade makes Bub3p an outlier when compared to other structurally determined WD40 proteins.

Bub3 proteins from other organisms also deviate at key residues of the WD40 signature sequence. Although many contain the common WD pair in blades 3, 4 and 6 (Figure 1), the tryptophan side chains probably do not participate in the triad

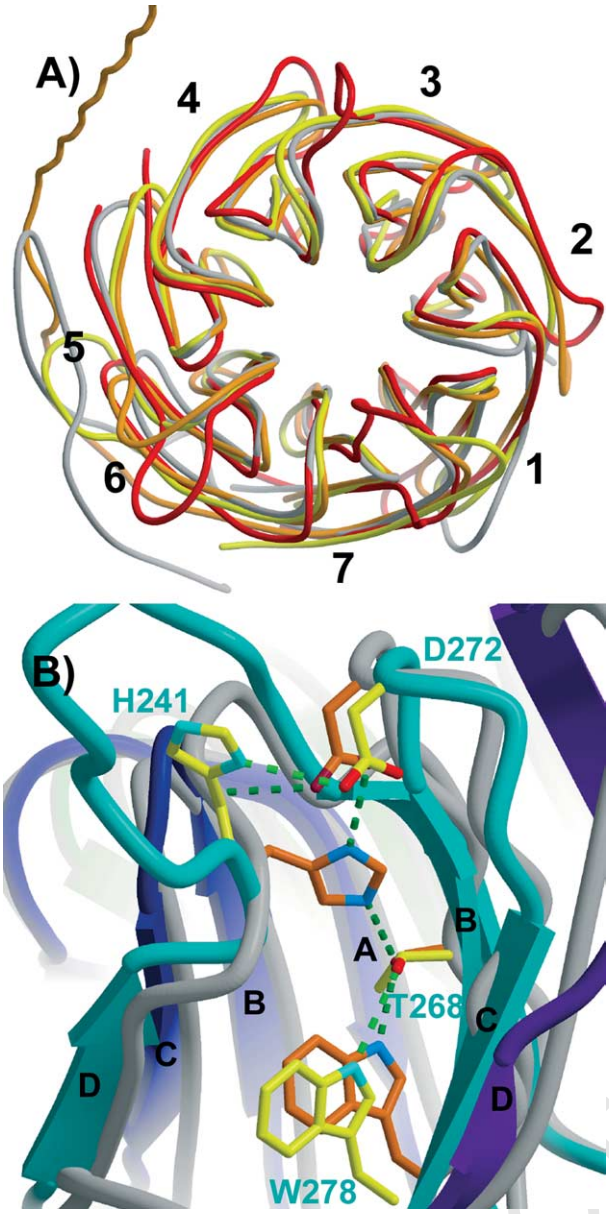

Figure 3. Superposition of Bub3p. (A) Superposition of Bub3p in red, transducin Gβ in orange (PDB accession 1GOT).[37] β-TrCP1 in yellow (PDB 1P22),[41] and Groucho1-tle co-repressor in gray (PDB 1GXR).[47] High conservation is observed in the strands with diversity located at insertions at the termini and the loop regions. The molecules were superimposed according to rotation and translation matrices derived from the algorithm employed by DALI.[35] (B) Superposition of the prototypic WD-40 structural triad from Groucho1-tle blade 6 (gray) and Bub3p blade6. The secondary structure of Bub3 is shown and the pertinent side chains are colored in lighter shades, while the corresponding side chains of Groucho1 are shown in muted tones. Broken lines represent H-bonds.

hydrogen bonding network, as mapping the aligned sequences to the assigned secondary structure of Bub3p shows that the requisite Ser/Thr and His residues are absent.

Loop insertions

A typical WD40 repeat contains approximately 40 amino acid residues, but loop insertions are common.[36–39] Repeats in Bub3p vary in length from 41 to 62 amino acid residues. Many of the loops have short insertions instead of the 3-residue tight turns seen, for example, in the transducin Gβ structure.[37] Inspection of Bub3 sequence alignments reveals that these insertions are not strictly conserved in sequence or in length. Indeed, the length and composition of the seven-residue insertion in the DA loop between blades 3 and 4 is unique (among listed sequences) to *S. cerevisiae* (Figure 1), as is the poorly ordered CD loop of blade 5 on the bottom face.

The most prominent loop insertions are in the DA loop between blades 5 and 6 (11 residues) and the BC loop within blade 7 (18 residues). These two loops extend 12 Å and 16 Å, respectively, from the top face of the propeller (C^{α} to C^{α}), creating a cleft with an opening of 10.5 Å at its narrowest point. The extended BC loop is well ordered, except for three residues at its tip. The amino-terminal end of this loop (residues 315–318) is a short, single-turn helix, one of only two such helical turns in the molecule (Figures 1 and 2(b)). The functional significance of the DA and BC loops is not evident, although their prominence is suggestive. Alignment of the sequences of all known and putative Bub3 homologs (Figure S1-supplement) shows that these loops have little sequence conservation and their length is variable, ranging from 11 to 15 residues for the DA loop and from 15 to 25 residues for the BC loop.

Characteristics of the molecular surface

A sequence variability score was assigned to each residue based on the alignment of 15 known and putative Bub3 homologs. This variability was subsequently mapped to the molecular surface (Figure 4(a)–(d)). There is a broad patch of high conservation on the top face of the molecule, extending in a stripe along the lateral face spanning blades 5 and 6 (Figure 4(a) and (b)). The bottom face and the remainder of the molecular perimeter (blades 1–4 and 7) are noticeably less conserved (Figure 4(c) and (d)). The conserved surface on the top face of the molecule is relatively hydrophobic, but a number of basic residues, especially within the mouth of the central tunnel, make it electropositive. The conserved surface along the side has a mixed electrostatic potential (Figure 4(e) and (f)).

Several mutants have been reported that map to the conserved surface regions.[8,10] The single W31G and W120G mutants do not co-immunoprecipitate with Mad2/Mad3/Cdc20, presumably due to disruption of the mitotic checkpoint complex (MCC).[10] The single mutants grow normally in benomyl, however, indicating that the checkpoint is functional. In contrast, the double mutant is sensitive to

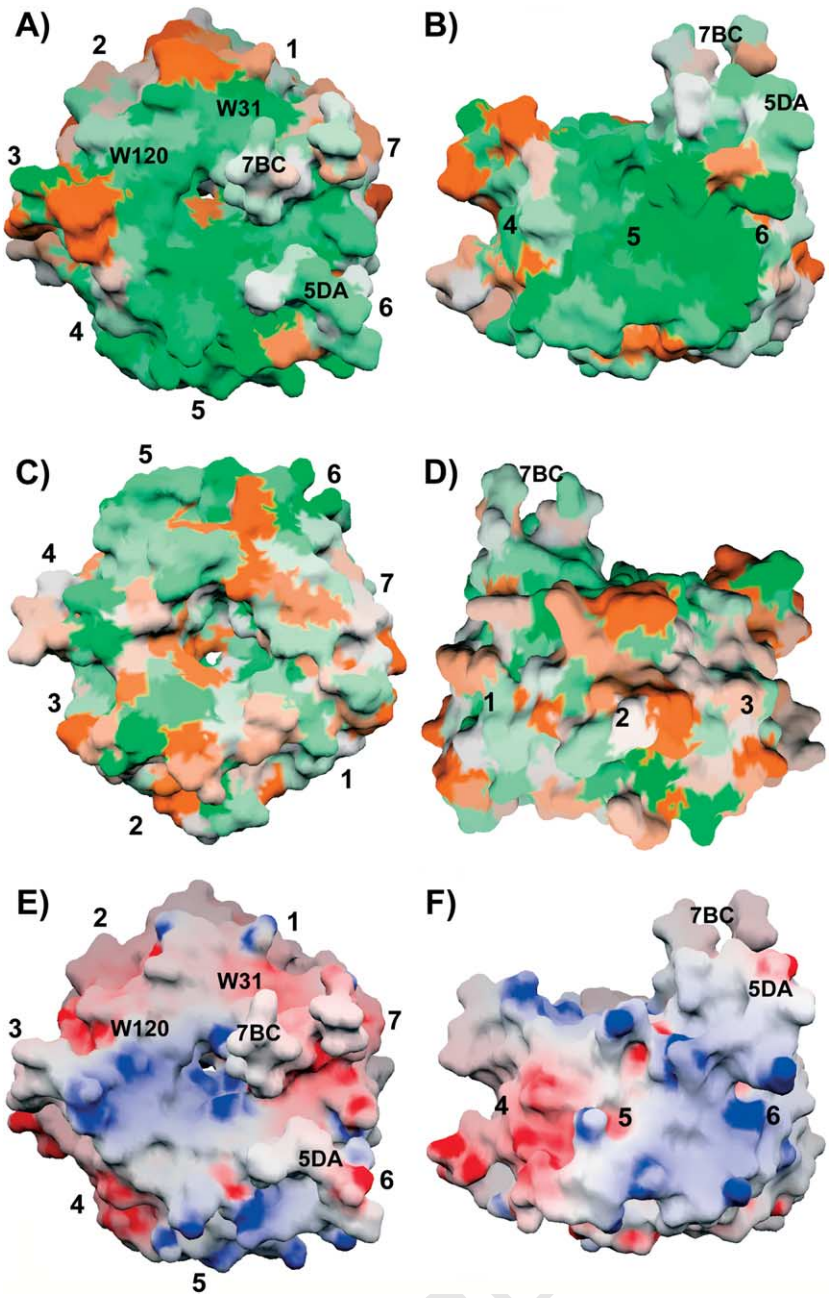

Figure 4. Conserved and electrostatic surfaces. (A) Top face. (B) 90° Side face. (C) Bottom face. (D) Side face, 180° relative to B. In the top four panels, sequences from 15 known and putative Bub3 homologs were aligned and scored according their sequence conservation. This score was scaled and used to color the molecular surface such that green and orange surfaces correspond to conserved and divergent regions, respectively. The approximate location of the blades is indicated by numbers; the locations of conserved W31 and W120 and the prominent surface loops are also labeled. (E) Top view. (F) Side view. In the bottom panels, the electrostatic potential is mapped to the conserved molecular surface (identical orientations to A and B). In this coloring scheme, red and blue surfaces correspond to negative and positive electrostatic potential scaled from $-20\,k_bT$ to $20\,k_bT$, respectively. This figure was generated with GRASP.[48]

benomyl, with a slow growth phenotype similar to that of bub3Δ cells.[10] These conserved tryptophans, located in blades 1 and 3 immediately before the Asp at the tip of the BC loop, form an extended hydrophobic platform on the top surface of the molecule. Deletion of the conserved VAVE sequence in the βC strand in blade 5 of human Bub3 (residues 218–221) (Figure 1) results in a mutant that no longer localizes to the kinetochore, but remains nuclear and fails to co-localize in the cytoplasm with Bub1 or BubR1 (Mad3 homolog).[8] This VAVE sequence lies on the conserved lateral stripe, and the deletion would disrupt its surface (Figure 4(b)). Thus, the published mutational data support the notion that these surfaces of Bub3 are key interaction points for additional components of the spindle checkpoint, presumably Bub1 and Mad3/BubR1.

Binding partners

The proposed sites along the top face and between blades 5 and 6 are consistent with other observed WD40 binding modes.[37,38,40,41] In some cases, for example the interaction of transducin Gβ with Gα,[37] the partner is a folded domain that presents a complementary surface to the top of the propeller. In others, the partner is a segment of polypeptide chain that extends along or across the propeller in the bound state but that is unstructured on its own.[38,40,41] Mad3 and Bub1 contain a conserved stretch of about 45 amino acid residues (315–356 in Bub1 and 354–401 in Mad3), which has been identified as the Bub3 binding site.[8,9] These elements are probably too short to have independent folded structures, and the conserved surface on Bub3 probably provides an extended template

for folding the target segment. Secondary-structure predictions suggest β-conformation toward the N terminus of the 45-residue sequence and an α-helix toward the C terminus.[42] Formation and regulation of this interaction are likely to be important aspects of checkpoint signaling.

Comparison to mRNA export factor Rae1

Bub3 has substantial sequence similarity with the protein Ra1; the two have 26% identity and 42% similarity in yeast, and 34% identity and 52% similarity in humans (Figure S2—supplement). Several lines of evidence support the hypothesis that Rae1 (also called Gle2) associates with mRNP complexes to facilitate their export from the nucleus.[43] Rae1 binds the nuclear pore complex through a short, so-called GLEBS motif (*Gle*2p-binding-sequence); Mad3 and Bub1 also contain a GLEBS motif, which falls within the region that has been implicated in Bub3 binding.[43] While Bub3 binding appears to be specific for Mad3 and Bub1, Rae1 appears to be relatively non-specific, binding the nuclear pore complex as well as Bub1. The interaction between Bub1 and Rae1 may have a specific or perhaps redundant role in the spindle checkpoint; Bub3 or Rae1 haplo-insufficiency in mice have similar phenotypes exhibiting spindle checkpoint and chromosome segregation defects.[6] Moreover, overexpression of Rae1 complements Bub3 haplo-insufficiency in mice.[6] The sequence alignment of Rae1 with Bub3 shows conserved residues located along the top surface of the propeller and the lateral surface spanning blades 5–6. The two conserved Trp residues on the top surface of Bub3, which are implicated in Bub1 and Mad3 binding, are likewise conserved in Rae1. Therefore, Rae1 and Bub3 probably interact with Bub1 in a very similar way.

Coordinates

The atomic coordinates for Bub3p and structure factors have been deposited for immediate release in the Protein Data Bank with accession code 1U4C.

Acknowledgements

We thank Katya Heldwein, Piotr Sliz, and Eric Vogan for discussions on phasing and refinement strategies. NAL acknowledges a postdoctoral fellowship from the Jane Coffin Childs Memorial Fund for Medical Research; SCH is an Investigator in the Howard Hughes Medical Institute.

Supplementary data

Supplementary data associated with this article can be found at doi:10.1016/j.jmb.2004.09.094

References

1. Rieder, C. L., Schultz, A., Cole, R. & Sluder, G. (1994). Anaphase onset in vertebrate somatic cells is controlled by a checkpoint that monitors sister kinetochore attachment to the spindle. *J. Cell Biol.* **127**, 1301–1310.
2. Li, X. & Nicklas, R. B. (1995). Mitotic forces control a cell-cycle checkpoint. *Nature*, **373**, 630–632.
3. Yu, H. (2002). Regulation of APC-Cdc20 by the spindle checkpoint. *Curr. Opin. Cell Biol.* **14**, 706–714.
4. Hoyt, M. A., Totis, L. & Roberts, B. T. (1991). *S. cerevisiae* genes required for cell cycle arrest in response to loss of microtubule function. *Cell*, **66**, 507–517.
5. Kalitsis, P., Earle, E., Fowler, K. J. & Choo, K. H. A. (2000). Bub3 gene disruption in mice reveals essential mitotic spindle checkpoint function during early embryogenesis. *Genes Dev.* **14**, 2277–2282.
6. Babu, J. R., Jeganathan, K. B., Baker, D. J., Wu, X., Kang-Decker, N. & van Deursen, J. M. (2003). Rae1 is an essential mitotic checkpoint regulator that cooperates with Bub3 to prevent chromosome missegregation. *J. Cell Biol.* **160**, 341–353.
7. Roberts, B. T., Farr, K. A. & Hoyt, M. A. (1994). The *Saccharomyces cerevisiae* checkpoint gene Bub1 encodes a novel protein kinase. *Mol. Cell Biol.* **14**, 8282–8291.
8. Taylor, S. S., Ha, E. & McKeon, F. (1998). The human homologue of Bub3 is required for kinetochore localization of Bub1 and a Mad3/Bub1-related kinase. *J. Cell Biol.* **142**, 1–11.
9. Hardwick, K. G., Johnston, R. C., Smith, D. L. & Murray, A. W. (2000). Mad3 encodes a novel component of the spindle checkpoint which interacts with Bub3, Cdc20, and Mad2. *J. Cell Biol.* **148**, 871–882.
10. Fraschini, R., Beretta, A., Sironi, L., Musacchio, A., Lucchini, G. & Piatti, S. (2001). Bub3 interaction with Mad2, Mad3 and Cdc20 is mediated by WD40 repeats and does not require intact kinetochores. *EMBO J.* **20**, 6648–6659.
11. Hunter, T. & Plowman, G. D. (1997). The protein kinases of budding yeast: six score and more. *Trends Biochem. Sci.* **22**, 18–22.
12. Tang, Z., Bharadwaj, R., Li, B. & Yu, H. (2001). Mad2-independent inhibition of APC-CDC20 by the mitotic checkpoint protein BubR1. *Dev. Cell*, **1**, 227–237.
13. Sudakin, V., Chan, G. K. & Yen, T. J. (2001). Checkpoint inhibition of the APC/C in HeLa cells is mediated by a complex of BubR1, Bub3, Cdc20, and Mad2. *J. Cell Biol.* **154**, 925–936.
14. Fang, G. (2002). Checkpoint protein BubR1 acts synergistically with Mad2 to inhibit anaphase-promoting complex. *Mol. Biol. Cell*, **13**, 755–766.
15. Taylor, S. S. & McKeon, F. (1997). Kinetochore localization of murine Bub1 is required for normal mitotic timing and checkpoint response to spindle damage. *Cell*, **89**, 727–735.
16. Kerscher, O., Crotti, L. B. & Basrai, M. A. (2003). Recognizing chromosomes in trouble: association of the spindle checkpoint protein bub3p with altered kinetochores and a unique defective centromere. *Mol. Cell Biol.* **23**, 6406–6418.
17. Gillett, E. S., Espelin, C. W. & Sorger, P. K. (2004). Spindle checkpoint proteins and chromosome-microtubule attachment in budding yeast. *J. Cell Biol.* **164**, 1–12.
18. Janke, C., Ortiz, J., Lechner, J., Shevchenko, A., Magiera, M. M., Schramm, C. & Schiebel, E. (2001).

The budding yeast proteins Spc24p and Spc25p interact with Ndc80p and Nuf2p at the kinetochore and are important for kinetochore clustering and checkpoint control. *EMBO J.* **21**, 181–193.
19. McCleland, M. L., Gardner, R. D., Kallio, M. J., Daum, J. R., Gorbsky, G. J., Burke, D. J. & Stukenberg, P. T. (2003). The highly conserved Ndc80 complex is required for kinetochore assembly, chromosome congression, and spindle checkpoint activity. *Genes Dev.* **17**, 101–114.
20. Martin-Lluesma, S., Stucke, V. M. & Nigg, E. A. (2002). Role of Hec1 in spindle checkpoint signaling and kinetochore recruitment of Mad1/Mad2. *Science*, **297**, 2267–2270.
21. DeLuca, J. G., Howell, B. J., Canman, J. C., Hickey, J. M., Fang, G. & Salmon, E. D. (2003). Nuf2 and Hec1 are required for retention of the checkpoint proteins Mad1 and Mad2 to kinetochores. *Curr. Biol.* **13**, 2103–2109.
22. Howell, B. J., Moree, B., Farrar, E. M., Stewart, S., Fang, G. & Salmon, E. D. (2004). Spindle checkpoint protein dynamics at kinetochores in living cells. *Curr. Biol.* **14**, 953–964.
23. Shah, J. V., Botvinick, E., Bonday, Z., Furnari, F., Berns, M. & Cleveland, D. W. (2004). Dynamics of centromere and kinetochore proteins: implications for checkpoint signaling and silencing. *Curr. Biol.* **14**, 942–952.
24. Otwinowski, Z. & Minor, W. (1997). Processing of X-ray diffraction data collected in oscillation mode. *Methods Enzymol.* **276**, 307–326.
25. Terwilliger, T. C. & Berendzen, J. (1997). Bayesian MAD phasing. *Acta Crystallog. sect. D*, **53**, 571–579.
26. Bricogne, G., Vonrhein, C., Flensburg, C., Schiltz, M. & Paciorek, W. (2003). Generation, representation and flow of phase information in structure determination: recent developments in and around SHARP 2.0. *Acta Crystallog. sect. D*, **59**, 2023–2030.
27. Abrahams, J. P. & Leslie, A. G. W. (1996). *Acta Crystallog. sect. D*, **52**, 30–42.
28. Cowtan, K. D. & Main, P. (1996). Phase combination and cross validation in iterated density-modification calculations. *Acta Crystallog. sect. D*, **52**, 43–48.
29. Jones, T. A., Zou, J. Y., Cowan, S. W. & Kjeldgaard, M. (1991). Improved methods for building protein models in electron density maps and the location of errors in these models. *Acta Crystallog. sect. A*, **47**, 110–119.
30. Brünger, A. T., Adams, P. D., Clore, G. M., Delano, W. L., Gros, P., Grosse-Kunstleve, R. W. *et al.* (1998). Crystallography and NMR system: a new software suite for molecular structure determination. *Acta Crystallog. sect. D*, **54**, 905–921.
31. Yeates, T. O. (1997). Detecting and overcoming crystal twinning. *Methods Enzymol.* **276**, 344–358.
32. Sheldrick, G. M. & Schneider, T. R. (1997). SHELXL: high-resolution refinement. *Methods Enzymol.* **277B**, 319–343.
33. Herbst-Irmer, R. & Sheldrick, G. M. (1998). Refinement of twinned structures with SHELXL97. *Acta Crystallog. sect. B*, **54**, 443–449.
34. Larsen, N. A., Heine, A., de Prada, P., Redwan, R. M., Yeates, T. O., Landry, D. W. & Wilson, I. A. (2002). Structure determination and refinement of a cocaine hydrolytic antibody from a pseudomerohedrally twinned crystal. *Acta Crystallog. sect. D*, **58**, 2055–2059.
35. Holm, L. & Sander, C. (1993). Protein structure comparison by alignment of distance matrices. *J. Mol. Biol.* **233**, 123–138.
36. Neer, E. J., Schmidt, C. J., Nambudripad, R. & Smith, T. F. (1994). The ancient regulatory-protein family of WD-repeat proteins. *Nature*, **371**, 297–300.
37. Sondek, J., Bohm, A., Lambright, D. G., Hamm, H. E. & Sigler, P. B. (1996). Crystal structure of a G-protein bg dimer at 2.1 Å resolution. *Nature*, **379**, 369–374.
38. Haar, t.-E., Harrison, S. C. & Kirchhausen, T. (2000). Peptide-in-groove interactions link target proteins to the b-propeller of clathrin. *Proc. Natl Acad. Sci. USA*, **97**, 1096–1100.
39. Sprague, E. R., Redd, M. J., Johnson, A. D. & Wolberger, C. (2000). Structure of the C-terminal domain of Tup1, a corepressor of transcription in yeast. *EMBO J.* **19**, 3016–3027.
40. Orlicky, S., Tang, X., Willems, A., Tyers, M. & Sicheri, F. (2003). Structural basis for phosphodependent substrate selection and orientation by the SCF^Cdc4 ubiquitin ligase. *Cell*, **112**, 243–256.
41. Wu, G., Xu, G., Schulman, B. A., Jeffrey, P. D., Harper, J. W. & Pavletich, N. P. (2003). Structure of a b-TrCP1-Skp1-b-catenin complex: destruction motif binding and lysine specificity of the SCF^b-TrCP1 ubiquitin ligase. *Mol. Cell*, **111**, 1445–1456.
42. Rost, B. (1996). *Methods Enzymol.* **266**, 525–539.
43. Wang, X., Babu, J. R., Harden, J. M., Jablonski, S. A., Gazi, M. H., Lingle, W. L. *et al.* (2001). The mitotic checkpoint protein hBub3 and the mRNA export factor hRae1 interact with GLE2p-binding sequences (GLEBS)-containing proteins. *J. Biol. Chem.* **276**, 26559–26567.
44. Thompson, J. D., Higgins, D. G. & Gibson, T. J. (1994). CLUSTAL W: improving the sensitivity of progressive multiple sequence alignment through sequence weighting, position-specific gap penalties and weight matrix choice. *Nucl. Acids Res.* **22**, 4673–4680.
45. Esnouf, R. M. (1999). Further additions to MOLSCRIPT version 1.4, including reading and contouring of electron density maps. *Acta Crystallog. sect. D*, **55**, 938–940.
46. Merritt, E. A. & Murphy, M. E. P. (1994). Raster3D Version 2.0. A program for photorealistic molecular graphics. *Acta Crystallog. sect. D*, **50**, 869–873.
47. Pickles, L. M., Roe, S. M., Hemingway, E. J., Stifani, S. & Pearl, L. H. (2002). Crystal structure of the C-terminal WD40 repeat domain of the human Groucho-TLE1 transcriptional corepressor. *Structure*, **10**, 751–761.
48. Nichols, A., Sharp, K. A. & Honig, B. (1991). Protein folding and association: insights from the interfacial and thermodynamic properties of hydrocarbons. *Proteins: Struct. Funct. Genet.* **11**, 281–296.

Edited by I. Wilson

(Received 23 July 2004; received in revised form 27 September 2004; accepted 29 September 2004)